ADVANCED SCIENCE Open Access
www.advancedscience.com

Highly Selective CO_2 Reduction to Pure Formic Acid Using a Nafion-TiO_2 Composite Porous Solid Electrolyte

*Yeomin Kang, Kooyoung Jung, Jusung Kim, and Ki Tae Park**

The electrochemical reduction of CO_2 (CO_2RR) to liquid fuels and chemicals offers a sustainable route to close the carbon cycle. Solid-state electrolyte (SSE) systems have recently emerged as a breakthrough platform, enabling the direct synthesis of high-purity liquid products. Here, a novel Nafion-based porous solid electrolyte (NPSE) with tunable thickness and porosity is presented, replacing conventional bead-type ion-exchange resins. The structural tunability of NPSEs plays a critical role in determining CO_2RR performance. Furthermore, a Nafion-titanium dioxide (TiO_2) composite NPSE (NPSE-TiO_2) is developed, in which TiO_2 nanoparticles significantly enhance the selectivity and productivity of formic acid. The NPSE-TiO_2 achieves a record-high Faradaic efficiency (FE_{HCOOH}) of 98.6%, the highest value reported to date among SSE systems, along with a high partial current density (j_{HCOOH}) of 431.8 mA cm^{-2}, yielding electrolyte-free formic acid with a single-pass concentration of 17.4 wt.%. Mechanistic investigations reveal that TiO_2 promotes the transport of formate anions ($HCOO^-$), suppressing back-diffusion of formic acid to the cathode and stabilizing cathodic pH.

1. Introduction

The increasing atmospheric concentration of CO_2 due to fossil fuel combustion and industrial activities has heightened the urgency of developing carbon capture and utilization (CCU) technologies.[1] Among various electrochemical CO_2 reduction reaction (CO_2RR) products, formic acid (HCOOH) is particularly attractive due to its high energy density, liquid-phase storage capability, and use as both a hydrogen carrier and a key industrial chemical. Compared to gaseous products such as carbon monoxide, formic acid offers distinct advantages in handling, storage, and transportation due to its liquid phase at ambient conditions, making it a highly promising candidate for sustainable energy and chemical production. However, a major challenge in formic acid production via CO_2RR is that the reaction often takes place in alkaline or neutral conditions, leading to the formation of formate salts mixed with electrolyte rather than free formic acid.[2–16] This necessitates additional downstream purification and acidification steps, increasing process complexity and energy requirements.[17,18] To address this challenge, Yang et al. introduced a solid-state electrolyte (SSE) system for a CO_2RR electrolyser, which consisted of three distinct compartments separated by an anion exchange membrane and a cation exchange membrane. This configuration enabled the direct production of high-purity formic acid; however, it suffered from relatively low product selectivity and current density.[19] Since then, various research groups have developed increasingly advanced catalyst designs to improve the Faradaic efficiency and current density of CO_2RR.[20–27] In addition, the SSE system design has been expanded to the production of other value-added products. For example, Wi et al. demonstrated that the SSE cell configuration enables the production of C_2 products,[28] while Xia et al. and Zhang et al. reported promising results for oxygen reduction for hydrogen peroxide production.[29,30] Additionally, Liu et al. have incorporated SSE cell configurations in the particularly difficult electrochemical synthesis of urea.[31] Despite these advances, the solid electrolyte system still suffers from high overall cell voltages, reducing energy efficiency compared to conventional electrochemical setups.[18,32]

While most studies focus on catalyst development to improve selectivity and activity, the design and operation of the electrolysis cell themselves play equally crucial roles in achieving efficient CO_2RR. Among the various cell components, SSE materials have been identified as a major source of internal resistance, leading to high cell voltages.[22] Optimizing the architecture and physicochemical properties of SSEs may provide a more cost-effective and scalable strategy for reducing energy losses and improving overall process efficiency. Recently, Cherniack et al. introduced an ionomer wafer to further investigate the interfacial phenomena between components of the SSE cell.[33] However, this design exhibited low selectivity toward CO_2RR products due to insufficient anion transport and back-diffusion of produced formic acid to the cathode, leading to product loss from the center compartment and a decrease in selectivity of CO_2RR due to local acidification, which promotes the hydrogen evolution reaction (HER).

Y. Kang, K. Jung, J. Kim, K. T. Park
Department of Chemical Engineering
Konkuk University
120 Neungdong-ro, Gwangjin-gu, Seoul 05029, Republic of Korea
E-mail: kpark@konkuk.ac.kr

The ORCID identification number(s) for the author(s) of this article can be found under https://doi.org/10.1002/advs.202515967

© 2025 The Author(s). Advanced Science published by Wiley-VCH GmbH. This is an open access article under the terms of the Creative Commons Attribution License, which permits use, distribution and reproduction in any medium, provided the original work is properly cited.

DOI: 10.1002/advs.202515967

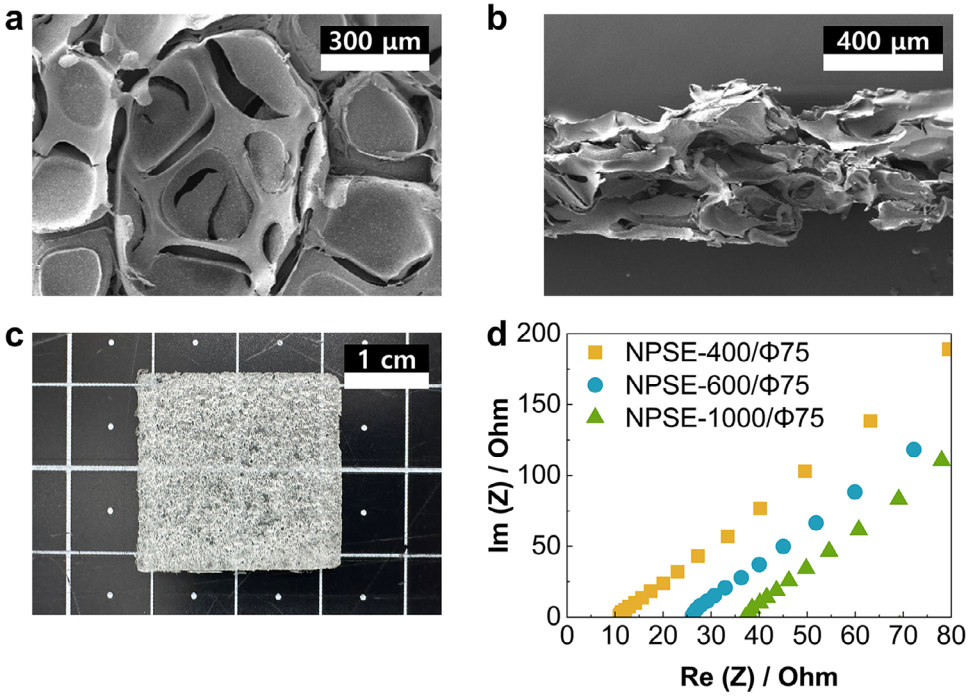


Figure 1. Morphological and electrochemical characterization of NPSE samples. a) Top-view and b) cross-sectional SEM images of NPSE-600/Φ75, revealing a well-defined porous structure. c) Digital photograph of NPSE-600/Φ75. d) Nyquist impedance plots (1 MHz to 100 Hz, E_{OC}, 10 mV amplitude) for isolated NPSE samples according to thickness.

Herein, we report a Nafion-based porous solid electrolyte (NPSE) as an advanced SSE platform for CO_2RR to formic acid. Through systematic optimization of the key parameters of NPSE, including thickness, porosity, and chemical composition, it was successfully verified that the NPSE design improvements can be as impactful as catalyst innovations, offering a practical and cost-effective pathway for advancing CO_2RR technologies. Beyond structural tuning, we further explore the incorporation of titanium dioxide (TiO_2) nanoparticles into the NPSE matrix as a strategy to enhance ionic properties and address limitations associated with formate anion transport and back-diffusion of formic acid. This study highlights the importance of solid electrolyte engineering in advancing SSE systems capable of high selectivity, improved energy efficiency, and scalable production of high-purity formic acid.

2. Results and Discussion

NPSEs were prepared via a metal foam leaching method, as shown in Figure S1 (Supporting Information). The prepared NPSEs were a continuous mesh of ionomers, forming a translucent, sponge-like gel having regular pores of ≈500 µm (**Figure 1**a–c). Various strategies have been explored to introduce porosity into Nafion membranes, including the use of volatile porogenes[34,35] and salting out techniques.[36,37] However, these conventional methods often fail to produce open-pore structures capable of supporting sufficient liquid flow, an essential requirement for the efficient recovery of liquid products in SSE systems. In contrast, our metal foam leaching method enables the reliable fabrication of porous solid electrolytes with well-defined open-pore architectures that facilitate effective and stable liquid transport throughout the solid electrolyte matrix.

The proposed method also enables precise control over key structural parameters of the NPSE, including thickness and porosity. The thickness was adjusted by varying the amount of ionomer dispersion injected, in combination with custom-fabricated polydimethylsiloxane (PDMS) wells and nickel foams (NF) with matched depth and thickness. NPSEs with target thicknesses of 400, 600, and 1000 µm were successfully fabricated (Figure S2, Supporting Information). Likewise, by tuning the porosity of the metal foam template, the porosity of the resulting NPSEs was adjusted to 75%, 60% and 50%, respectively (Figure S3, Supporting Information). With denser NFs, the resulting NPSEs had a closer-knit mesh, leading to a lower porosity solid electrolyte. The prepared NPSE samples were denoted as NPSE-thickness/porosity based on their thickness and porosity. For example, NPSE-600/Φ60 refers to a NPSE with a thickness of 600 µm and a porosity of 60%. A summary of the NPSE formulations and their structural characteristics is presented in Table S1 (Supporting Information). Further details on the preparation procedure are available in the Experimental Section of Supporting Information.

NPSE samples were characterized to elucidate their structural and compositional properties. As shown in Figure S4 (Supporting Information), scanning electron microscopy (SEM) for high-resolution imaging with energy-dispersive X-ray spectroscopy (EDS) revealed that the NPSE matrix was primarily composed of carbon, fluorene, and sulfur, consistent with the expected chemical composition of Nafion. Negligible amounts of nickel were detected by EDS (Table S2, Supporting Information), indicating

© 2025 The Author(s). Advanced Science published by Wiley-VCH GmbH

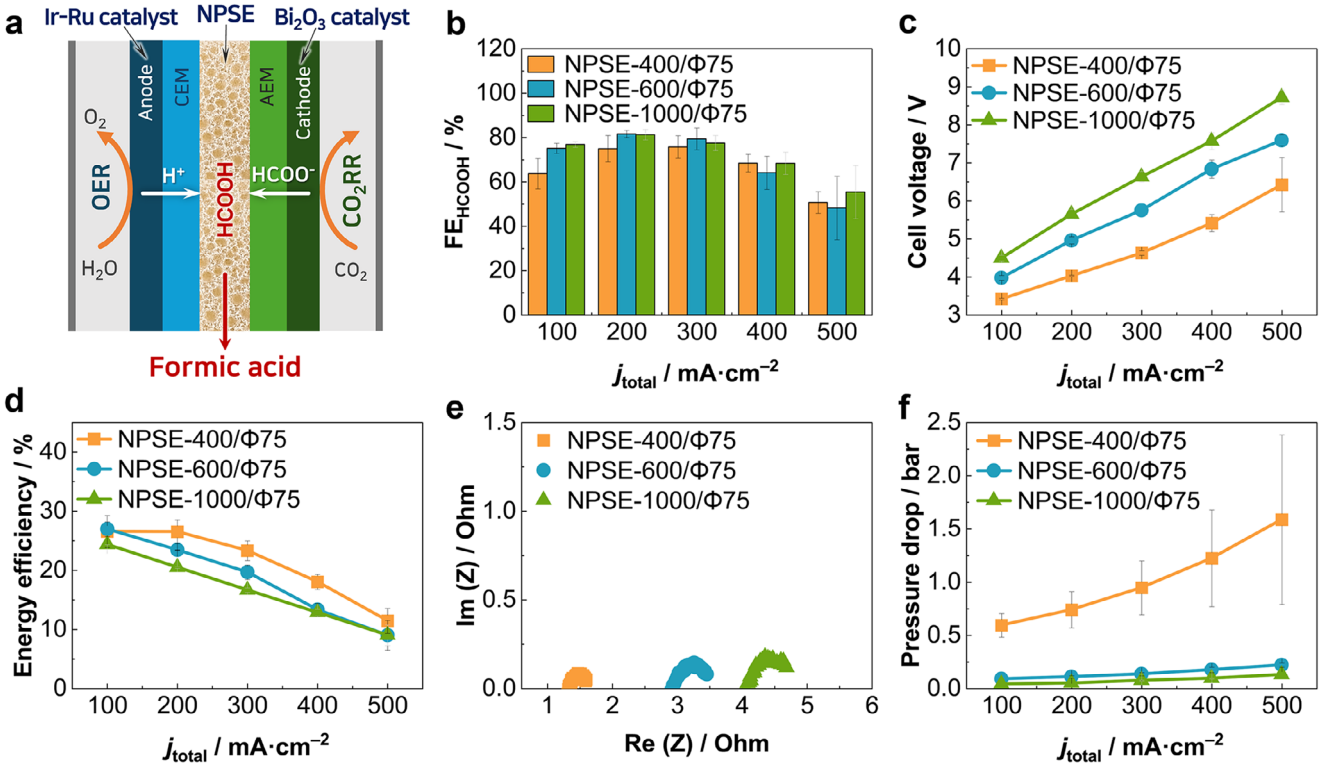


Figure 2. a) Schematic illustration of the solid-state electrolyte (SSE) cell employing Nafion-based porous solid electrolyte (NPSE). Performance metrics for CO_2RR as a function of NPSE thickness: b) Faradaic Efficiency (FE) for formic acid, c) full cell voltage, d) energy efficiency, e) Nyquist impedance plots (1 MHz to 10 Hz, 3.8V_{cell}, 30 mV amplitude), and f) pressure drop across the center compartment.

that the dilute piranha solution used was effective at removing the NF scaffold, while preserving the porous structure of the solid polymer electrolyte.

To evaluate the ion-conductive properties of the NPSEs, electrochemical impedance spectroscopy (EIS) measurements were carried out using a custom-designed solid electrolyte analysis cell (Figure S5, Supporting Information). As shown in Figure 1d, the solution resistance (R_S) increased with NPSE thickness, indicating higher proton transfer resistance due to the extended diffusion path. Notably, the R_S of NPSE-600/Φ60 was nearly identical to that of NPSE-400/Φ75 (Figure S6, Supporting Information), suggesting that both reducing thickness and lowering porosity are effective strategies for minimizing the ionic resistance of NPSEs.

In addition, the ion exchange capacity (IEC) of the NPSEs was measured via back titration (Figure S7, Supporting Information), with resulting IEC values of ≈0.9 meq mL^{-1}, which are consistent with the reported IEC of Nafion (0.83–1.02 meq g^{-1}).[38] These results, together with the aforementioned EDS analysis, confirm that the leaching process does not chemically degrade the Nafion ionomer, while effectively and completely removing the nickel foam scaffold.

To evaluate the CO_2RR performance, the fabricated NPSEs were introduced into the center compartment of solid-state electrolyte (SSE) cells, where the cathodic catalyst was commercially available bismuth oxide (Bi_2O_3) nanoparticles and the anode catalyst was a mix of iridium (Ir) and ruthenium (Ru) (**Figure 2a**). The cells were operated in an experimental setup as shown in Figure S8 (Supporting Information). CO_2RR performances were monitored using the chronopotentiometry (CP) technique, while electrochemical characteristics of the system were analyzed via EIS and linear sweep voltammetry (LSV). The structural parameters of the NPSEs and their correlation with CO_2 reduction performance were systematically investigated.

As the NPSE thickness increased from 400 to 1000 µm at a fixed porosity of 75%, the Faradaic efficiency (FE) for formic acid generally improved (Figure 2b). Among the tested samples, NPSE-600/Φ75 achieved the highest FE of 81.6% at a current density of 200 mA cm^{-2} (Figure 2b). Notably, the thickest sample, NPSE-1000/Φ75, demonstrated better selectivity at higher current densities above 400 mA cm^{-2} compared to that of thinner NPSEs. This enhancement in selectivity is attributed to the increased distance between the cathode and the acidic anode with thicker NPSE, which increases the local pH near the cathode and consequently suppresses the competing HER. Despite the improved CO_2RR selectivity observed with NPSE-1000/Φ75, the substantially higher cell voltage and resulting energy demand rendered the use of thicker NPSEs impractical for efficient CO_2RR, as shown in Figure 2c. A clear correlation was observed between NPSE thickness and cell voltage, with NPSE-1000/Φ75 exhibiting a high cell voltage of 8.72 V at 500 mA cm^{-2}.

When energy efficiency (EE), which accounts for both Faradaic efficiency (FE) and cell voltage, was used as a performance metric, NPSE-400/Φ75 consistently outperformed the thicker NPSEs, as shown in Figure 2d. This improvement is primarily attributed to reduced proton transport resistance in thinner NPSEs.

© 2025 The Author(s). Advanced Science published by Wiley-VCH GmbH

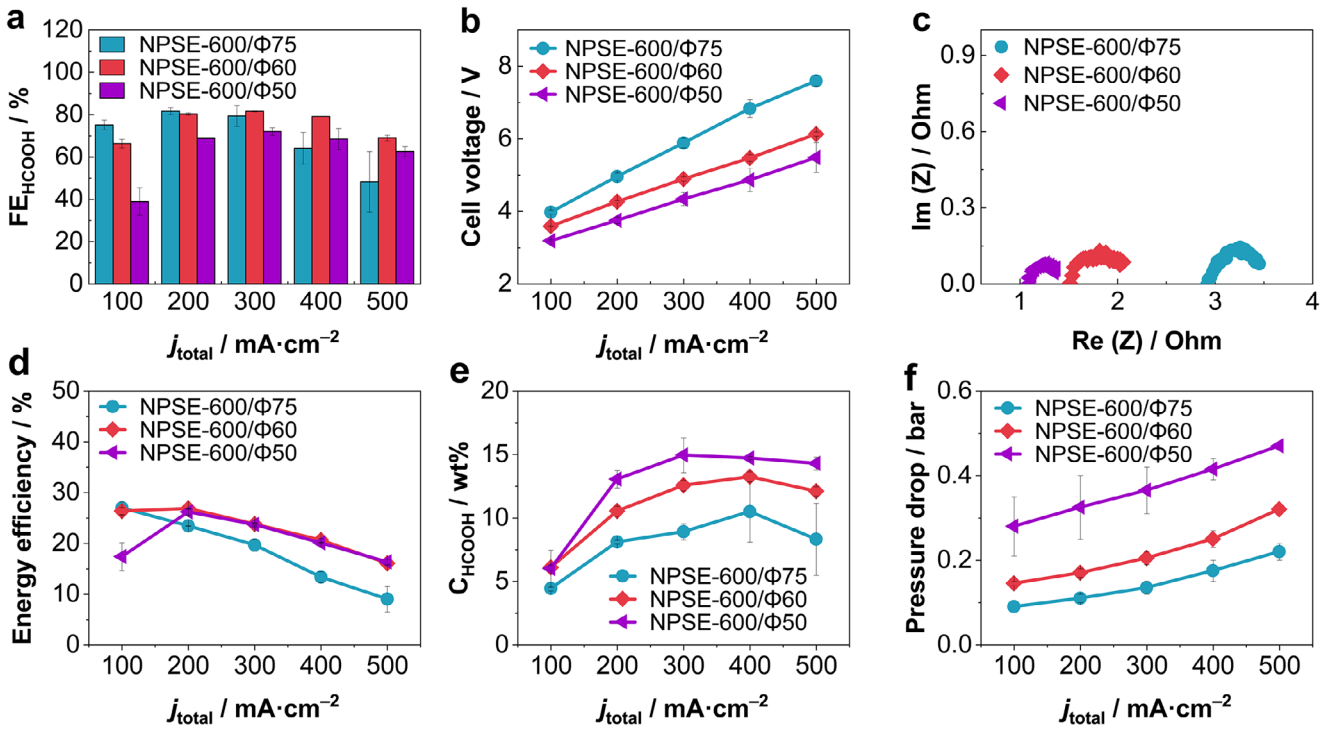


Figure 3. CO_2RR performance metrics as a function of NPSE porosity. a) Faradaic efficiency for formic acid (FE_{HCOOH}), b) Cell voltage, c) Nyquist impedance plots (1 MHz to 10 Hz, 3.8 V_{cell}, 30 mV amplitude), d) Energy efficiency (EE), e) Outlet concentrations of formic acid, and f) Pressure drop across the center compartment.

Nyquist plots (Figure 2e) further support this finding, revealing a substantial decrease in R_s and a moderate reduction in charge transfer resistance (R_{CT}) with decreasing NPSE thickness. Additionally, linear sweep voltammetry (LSV) results (Figure S9a, Supporting Information) showed that current density inversely correlated with NPSE thickness, supporting the trend of enhanced ionic conductivity and reduced resistance in thinner NPSE configurations.

However, although thinner NPSEs exhibited enhanced energy efficiency for formic acid production, excessive pressure drop was observed for NPSE-400/Φ75, especially at high current densities. At 500 mA cm^{-2}, the pressure drops across the center compartment reached ≈1.59 bar, as represented in Figure 2f. This significant increase of pressure drop with current density observed in NPSE-400/Φ75 is primarily attributed to the generation of CO_2 gas at increased current density.[19] Upon applying current to the SSE cell, hydronium ions (H_3O^+) are migrated from the anode, while a mixture of formate and carbonate/bicarbonate anions is delivered from the cathode into the center compartment through the cation exchange membrane (CEM) and anion exchange membrane (AEM), respectively. Within the acidic environment of the center compartment, the carbonate and bicarbonate species are rapidly converted to CO_2 gas, leading to volumetric expansion and a sharp increase in internal pressure. This excessive pressure drop compromised the operational stability of NPSE-400/Φ75, making it unsuitable for practical applications.

Interestingly, the outlet concentration of formic acid remained nearly constant across NPSEs of varying thickness (Figure S9b, Supporting Information). This behavior is attributed to a trade-off between pressure drop-induced flow resistance and residence time. In thinner NPSEs, although partial current densities were lower, the elevated pressure drop slowed liquid flow rate and increased residence time, resulting in comparable product concentrations. Considering these factors, particularly the severity of pressure-related limitations in thinner membranes and relatively low Faradaic efficiency, the 600 µm NPSE was selected as the minimum viable configuration for further investigation.

To investigate the influence of the porosity of NPSE on CO_2RR performance, a series of NPSEs with different porosities (Φ75, Φ60, and Φ50) but fixed thickness (600 µm) was evaluated in an SSE cell. As shown in **Figure 3a**, reducing the porosity from 75% to 60% led to significantly higher FE_{HCOOH} at higher current densities, with NPSE-600/Φ60 achieving 69.0% FE_{HCOOH} at 500 mA cm^{-2}, 22%p higher than NPSE-600/Φ75. However, when the porosity was further decreased to 50%, the FE_{HCOOH} dropped significantly compared to NPSE-600/Φ60. These results suggest that lowering porosity can be beneficial for reducing cell voltages at a given current density (Figure 3b), but overly dense NPSEs facilitate excessive proton transport at the NPSE/cathode interface, thereby accelerating HER.

The corresponding cell voltages presented in Figure 3b exhibit a clear trend of decreasing with reduced porosity at all current densities. This indicates a proportional decrease in internal resistance due to the denser structure of NPSE, which promotes ion transport. The EIS spectra (Figure 3c) and LSV curves (Figure S10, Supporting Information) further support this observation, showing decreasing ohmic resistance with increasing NPSE density.

© 2025 The Author(s). Advanced Science published by Wiley-VCH GmbH

Energy efficiency results are summarized in Figure 3d, where NPSE-600/Φ60 and NPSE-600/Φ50 clearly outperform the Φ75 sample across the entire tested current range, particularly at higher current densities. Except at 100 mA cm^{-2}, the NPSE-600/Φ60 and NPSE-600/Φ50 show comparable energy efficiency, as the decrease in cell voltage of the NPSE-600/Φ50 roughly offsetting the decrease in FE_{HCOOH}. These results highlight the importance of structural optimization in minimizing energy losses, an essential consideration for the practical scale-up of CO_2 electrolyzers.

The decrease in NPSE porosity led to an increase in the outlet concentration of formic acid (Figure 3e), with only a marginal increase in pressure drop of 0.07 and 0.24 bar for NPSE-600/Φ60 and NPSE-600/Φ50, respectively, compared to NPSE-600/Φ75 (Figure 3f). Unlike the case of varying NPSE thickness (Figure S9b, Supporting Information), this result is particularly notable because product concentration strongly impacts the economic viability of CO2RR, owing to the high costs of downstream separation and purification.[17,20,25] This correlation arises because decreasing NPSE porosity reduces internal void volume, thereby concentrating the generated formic acid within the transport pathways and leading to higher outlet product concentrations.

Interestingly, the cell resistance and corresponding operating cell voltage of NPSE-600/Φ60 were nearly identical to those of NPSE-400/Φ75. The only notable difference in CO_2RR performance between the two NPSEs was the pressure drops across the center compartment. The NPSE-600/Φ60 exhibited a significantly lower and more manageable maximum pressure drop of 0.32 bar (Figure 3f), compared to 1.59 bar for NPSE-400/Φ75, enabling more stable operation. These results suggest that optimizing porosity, rather than simply reducing thickness, is a more effective strategy for enhancing proton transport with maintaining hydrodynamic and operational stability. Hence, NPSEs were optimized to a thickness of 600 µm and porosity of 60%.

Following the identification of favorable structural parameters for NPSEs, CO_2RR performance was further enhanced by the incorporation of TiO_2 nanoparticles (TiO_2 NPs) into the NPSE matrix. As an amphoteric oxide, TiO_2 is known to function as both a Lewis and Brønsted acid.[39,40] Thus, its incorporation would increase the IEC of the solid electrolyte and further reduce ionic resistance. Uniform dispersion of TiO_2 NPs within the NPSE was achieved by blending TiO_2 slurry with Nafion dispersion with varying weight ratios (summarized in Table S3, Supporting Information). Successful incorporation was confirmed by SEM-EDS analysis (**Figure 4a**; Figures S11 and S12, Supporting Information), which also indicated complete removal of the Ni scaffold (Table S4, Supporting Information). All NPSE-TiO_2 composite samples were fabricated with a fixed thickness of 600 µm and a porosity of 60% (Figure S13, Supporting Information). The resulting NPSE-600/Φ60/TiO_2 maintained a similar morphology to unmodified NPSEs, except for a distinct opaque white coloration, as shown in Figure 4b.

The incorporation of TiO_2 into NPSE-600/Φ60 led to a notable enhancement in CO_2RR performance. As shown in Figure 4c, the FE_{HCOOH} reached 98.6% at 300 mA cm^{-2}, with a notably high selectivity of 86.4% maintained even at 500 mA cm^{-2}. This corresponded to a maximum partial current density of 431.8 mA cm^{-2} for formic acid production (Figure 4d). Additionally, TiO_2 incorporation also contributed to a reduction in cell voltage from 6.1 to 5.7 V at 500 mA cm^{-2} (Figure 4c). The synergetic effects of improved selectivity and reduced resistance led to a substantial improvement in energy efficiency and outlet concentration of formic acid, achieving values of 32.29% (Figure 4e) and 17.4 wt.% (Figure 4f), respectively.

EIS measurements (Figure 4g) showed that the incorporation of TiO_2 NPs led to a reduction in solution resistance (R_s), suggesting improved ionic transport. In addition, back titration measurements indicated up to a 75% increase in IEC compared to the unmodified NPSE-600/Φ60 with increasing TiO_2 loading (Figure S14 , Supporting Information). However, EIS results from both the SSE cells and isolated NPSE samples (Figures S15d and S16, Supporting Information) exhibited increased R_s at higher TiO_2 loadings. Moreover, the increase in IEC did not directly correlate with improvements in key CO_2RR performance metrics such as FE_{HCOOH}, cell voltage, j_{HCOOH}, or energy efficiency as shown in Figure S15 (Supporting Information). Among the tested samples, NPSE-600/Φ60/TiO_2 1% exhibited the highest CO_2RR performance. This suggests that beyond an optimal TiO_2 content, agglomeration of TiO_2 particles creates non-conductive domains that disrupt continuous ion transport pathways and increase overall resistance, thereby negating the benefits of enhanced IEC.

The operational stability of the NPSE-600/Φ60/TiO_2 1% was evaluated over 30 h at a constant current density of 200 mA cm^{-2} (Figure 4h). The cell maintained high selectivity (FE_{HCOOH} > 80%) and a stable operating cell voltage (≈4 V) throughout the test. Given the well-established mechanical and chemical robustness of Nafion and TiO_2, the promising long-term stability results are consistent with expectations.

However, the superior CO_2RR performance for formic acid production, particularly the substantial increase in the FE_{HCOOH}, achieved by NPSE-600/Φ60/TiO_2 1%, cannot be fully attributed to the increase in IEC or the reduction in R_s alone. To further investigate whether TiO_2 also affects the transport of formate anions ($HCOO^-$) within the NPSE, diffusion experiments were conducted using both a pristine Nafion membrane and a Nafion-TiO_2 composite membrane containing 1 wt.% TiO_2 NPs, as illustrated in Figure S17 (Supporting Information). Two chambers were separated by either a Nafion membrane or a Nafion-TiO_2 composite membrane, both of which were dense (non-porous) and cast to have a nominal thickness of 50 µm. The donor chamber was filled with 0.5 M potassium formate (HCOOK) solution, while the receiving chamber contained deionized water. Formate concentrations in the receiving chamber were monitored periodically over 1.5 h, and the resulting cumulative flux of $HCOO^-$ (µmol cm^{-2}) through each membrane is presented in **Figure 5a**.

Notably, the cumulative $HCOO^-$ flux through the Nafion-TiO_2 composite membrane reached 8.56 µmol cm^{-2} after 1.5 h, a 37.6% increase of that compared to pristine Nafion membrane (6.22 µmol cm^{-2}), as shown in Figure 5a. This result clearly indicates that the TiO_2 incorporation enhances $HCOO^-$ transport within the NPSE. To the best of our knowledge, this is the first reported evidence of TiO_2 facilitating formate transport when embedded in an ion-exchange membrane. Given that this enhancement was observed under purely diffusive conditions with a low concentration gradient (0.5 M), it is expected that $HCOO^-$ transport would be even more pronounced under practical operating conditions with higher concentration differentials exceeding 10 wt.% (Figure 4f).

© 2025 The Author(s). Advanced Science published by Wiley-VCH GmbH

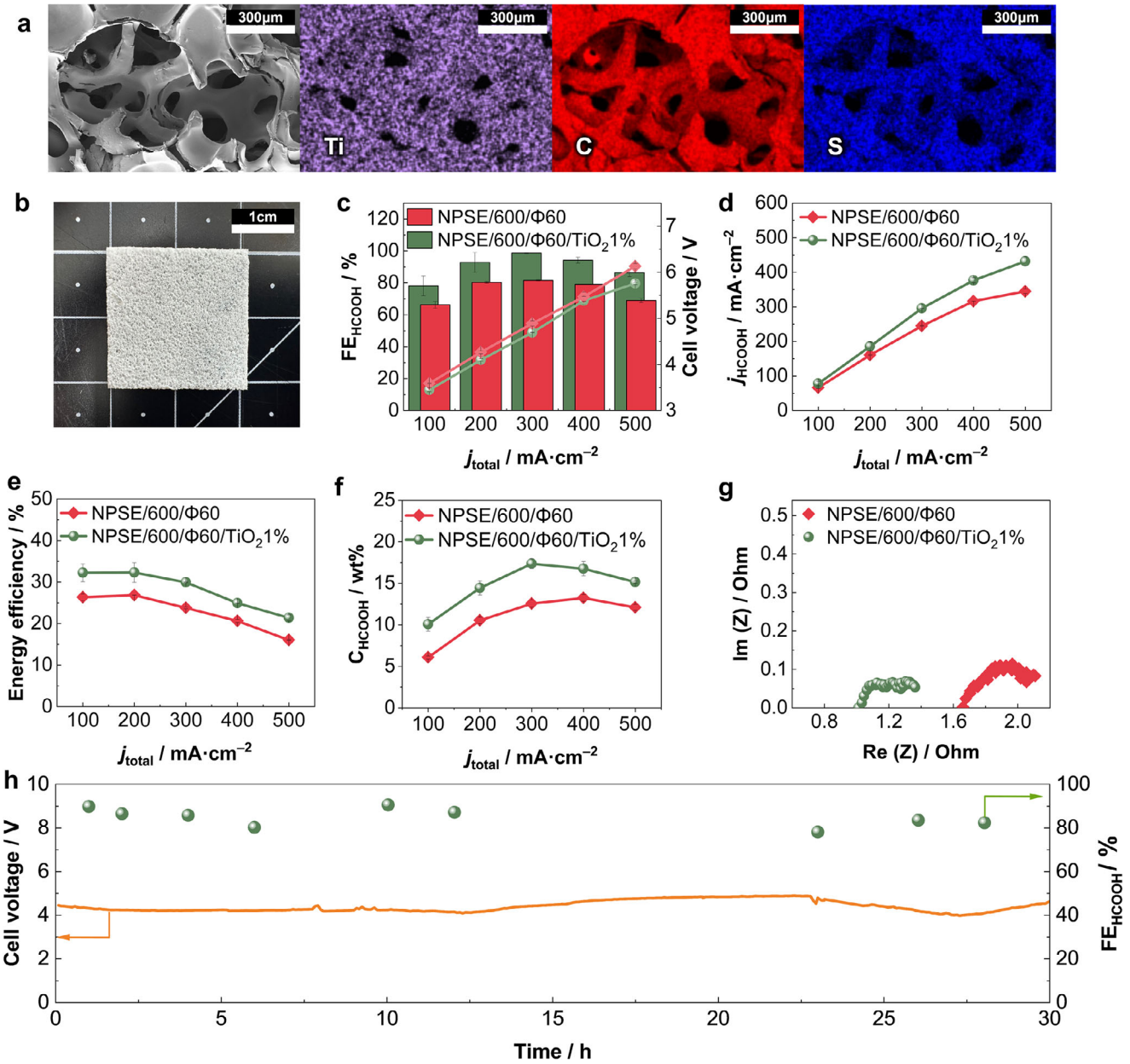


Figure 4. Characterization and CO_2RR performance of NPSE-600/Φ60/TiO_2 composite electrolytes. a) SEM-EDS mapping images of NPSE-600/Φ60/TiO_2 1%, showing uniform dispersion of Ti within the Nafion matrix (C and S). b) Digital photograph of NPSE-600/Φ60/TiO_2 1% sample. c) Faradaic efficiency for formic acid (FE_{HCOOH}), d) Partial current density for formic acid production (j_{HCOOH}), e) Energy efficiency, f) Outlet concentrations of formic acid, g) Nyquist impedance plots (1 MHz to 10 Hz, 3.8 V, 30 mV amplitude), and h) Long-term stablity test results using NPSE-600/Φ60/TiO_2 1% operating at 200 mA cm^{-2} over 30 h.

The mechanism by which TiO_2 facilitates formate anions is proposed to be adsorption-assisted transference. Formic acid is known to chemisorb on the surface of TiO_2 in monodentate and bidentate configurations.[41] To verify adsorption in the aqueous phase, a bulk adsorption experiment was conducted, in which a dilute solution of 85 μM HCOOK was treated with TiO_2 nanoparticles. As shown in Figure 5b, the HCOOK solution showed significant decreases in formate concentration (C_{HCOO^-}) after 30 min. The density of surface adsorption site was calculated to be 5.43 μmol m^{-2} (Table S5, Supporting Information), consistent with reported values (5≈6 μmol m^{-2}),[41] thereby providing strong evidence for the adsorption-assisted transference mechanism.

Crucially, the ability of the NPSE-TiO_2 composite to facilitate $HCOO^-$ transport not only effectively suppresses the back-diffusion of the produced formic acid but also improves the local pH environment at the cathode, both of which are critical for sustaining high CO_2RR selectivity. Previous studies have pointed to local pH and back diffusion being a significant factor in the CO_2RR selectivity of SSE systems.[32,42,43] Since the NPSE is composed of a cation-conductive Nafion ionomer, protons (H^+) are

© 2025 The Author(s). Advanced Science published by Wiley-VCH GmbH

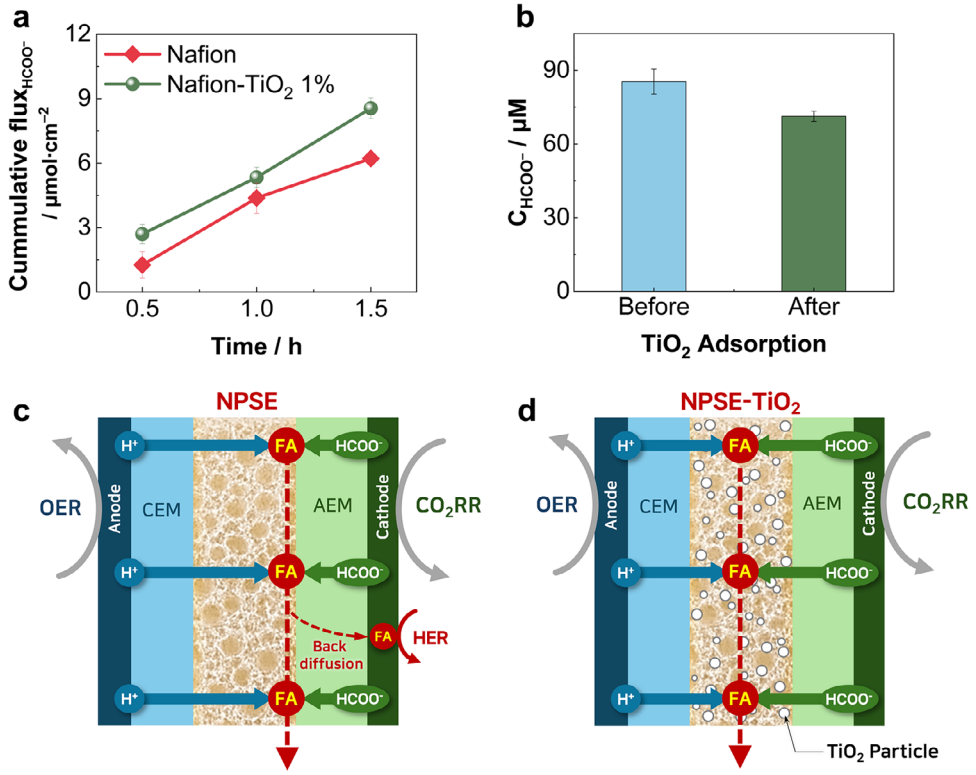


Figure 5. Mechanistic investigation of TiO_2 nanoparticle function in NPSE. a) Cumulative formate ion ($HCOO^-$) flux through either a pristine Nafion membrane or a Nafion-TiO_2 composite membrane. b) Formate concentrations of potassium formate solutions before and after TiO_2 treatment. c,d) Schematic illustrations of SSE cell operation: (b) without and (c) with TiO_2 nanoparticle incorporation.

readily transported through the NPSE, whereas formate anions ($HCOO^-$) are less likely to be transported. Consequently, the recombination of H^+ and $HCOO^-$ to form formic acid predominantly occurs at the NPSE-AEM interface near the cathode, as depicted in Figure 5b. In this configuration, the formic acid produced is susceptible to back-diffusion toward the cathode, leading to product loss from the center compartment and a decrease in FE_{HCOOH} due to local acidification, which promotes the HER.

In contrast, in the NPSE-TiO_2 composite, the incorporation of TiO_2 facilitates $HCOO^-$ transport, thereby shifting the site of formic acid formation farther from the cathode. This spatial displacement effectively mitigates back-diffusion of formic acid and sustains a more alkaline cathode environment, thereby enhancing CO_2RR selectivity. Therefore, these findings demonstrate that the incorporation of TiO_2 plays a crucial role in addressing key limitations of SSE cells, such as formic acid back-diffusion and low CO_2RR selectivity, by simultaneously enhancing IEC and anion transport, while stabilizing the local pH environment at the cathode.

3. Conclusion

In summary, we developed and systematically optimized Nafion-based porous solid electrolytes (NPSEs) for solid-state electrolyte (SSE) CO_2RR systems for the selective production of pure formic acid. Structural variables such as thickness, porosity, and TiO_2 incorporation were investigated to assess their impact on ion transport, selectivity, and energy efficiency. Our results show that NPSE thickness influences Faradaic efficiency, cell voltage, and energy efficiency, while porosity optimization further enhances system performance. Critically, the incorporation of 1 wt.% TiO_2 NPs into the NPSE matrix led to a dramatic improvement in formic acid selectivity (FE_{HCOOH} of up to 98.6%) with a high single-pass product concentration of 17.4 wt.% under electrolyte-free conditions. Mechanistic analyses revealed that TiO_2 not only increases the IEC and decreases ohmic resistance but also facilitates the transport of formate anions ($HCOO^-$). This improved $HCOO^-$ mobility was shown to suppress back-diffusion of formic acid and stabilize the local cathodic pH, which collectively enhanced CO_2RR selectivity. These findings highlight the importance of structural and compositional tuning in designing solid electrolytes for efficient CO_2RR. The NPSE-TiO_2 composite presents a promising platform for scalable, selective, and energy-efficient CO_2-to-formic acid conversion, offering insights for future development of advanced ion-conductive media. Future work should explore alternative ionomers and nanomaterials for SSE to further enhance ion transport and electrochemical performance.

Supporting Information

Supporting Information is available from the Wiley Online Library or from the author.

© 2025 The Author(s). Advanced Science published by Wiley-VCH GmbH

Acknowledgements

This work was financially supported by the Korea Evaluation Institute of Industrial Technology (KEIT) through the Alchemist Project (NTIS-2410005253, 20018904) through the Ministry of Trade, Industry and Energy (MOTIE, Korea), and by the National Research Foundation of Korea (NRF) grant funded by the Korean government (MSIT) (No.2022M3C1A3081432).

Conflict of Interest

The authors declare no conflict of interest.

Data Availability Statement

The data that support the findings of this study are available from the corresponding author upon reasonable request.

Keywords

CO_2 reduction, electrocatalysis, porous solid electrolyte, solid-state electrolyte, TiO_2

Received: August 20, 2025
Revised: September 23, 2025
Published online: October 13, 2025

[1] Z. Liu, Z. Deng, S. J. Davis, P. Ciais, *Nat. Rev. Earth Environ.* **2024**, *5*, 253.
[2] P. X. Lei, S. Q. Liu, Q. R. Wen, J. Y. Wu, S. Wu, X. Wei, R. Feng, X. Z. Fu, J. L. Luo, *Angew. Chem., Int. Ed.* **2025**, *64*, 202415726.
[3] L. P. Chi, Y. C. Zhang, Z. Z. Niu, X. L. Zhang, Y. C. Li, T. Y. Zhang, S. P. Sun, P. G. Lu, K. B. Tang, M. R. Gao, *Angew. Chem., Int. Ed.* **2025**, *64*, 202503539.
[4] J. Y. Li, J. R. Huang, Z. H. Zhao, H. L. Zhu, P. Q. Liao, X. M. Chen, *Angew. Chem., Int. Ed.* **2025**, *64*, 202511132.
[5] Y. Liu, Z. Wei, X. Su, X. Shi, L. Liu, T. Wang, X. Xu, M. Zhao, Y. Zhai, H. B. Yang, B. Liu, *Adv. Funct. Mater.* **2024**, *35*, 2403547.
[6] Z. Wei, J. Ding, Z. Wang, A. Wang, L. Zhang, Y. Liu, Y. Guo, X. Yang, Y. Zhai, B. Liu, *Angew. Chem., Int. Ed.* **2024**, *63*, 202402070.
[7] R. E. Siegel, M. Aceves, L. A. Berben, *ACS Energy Lett.* **2024**, *9*, 2896.
[8] S.-Q. Liu, M.-R. Gao, S. Wu, R. Feng, Y. Wang, L. Cui, Y. Guo, X.-Z. Fu, J.-L. Luo, *Energy Environ. Sci.* **2023**, *16*, 5305.
[9] Y. Liu, Z. Jiang, C. Huang, S. Jeong, A. L. Coughlin, S. Zhang, Y. Liu, X. Ye, *Nano Lett.* **2023**, *23*, 5911.
[10] L. P. Chi, Z. Z. Niu, Y. C. Zhang, X. L. Zhang, J. Liao, Z. Z. Wu, P. C. Yu, M. H. Fan, K. B. Tang, M. R. Gao, *Proc. Natl. Acad. Sci. USA* **2023**, *120*, 2312876120.
[11] K. Fernández-Caso, G. Díaz-Sainz, M. Alvarez-Guerra, A. Irabien, *ACS Energy Lett.* **2023**, *8*, 1992.
[12] D. Tan, W. Lee, Y. E. Kim, Y. N. Ko, M. H. Youn, Y. E. Jeon, J. Hong, J. E. Park, J. Seo, S. K. Jeong, Y. Choi, H. Choi, H. Y. Kim, K. T. Park, *ACS Appl. Mater. Interfaces* **2022**, *14*, 28890.
[13] L. P. Chi, Z. Z. Niu, X. L. Zhang, P. P. Yang, J. Liao, F. Y. Gao, Z. Z. Wu, K. B. Tang, M. R. Gao, *Nat. Commun.* **2021**, *12*, 5835.
[14] W. Lee, Y. E. Kim, M. H. Youn, S. K. Jeong, K. T. Park, *Angew. Chem., Int. Ed.* **2018**, *57*, 6883.
[15] S. Y. Choi, S. K. Jeong, H. J. Kim, I.-H. Baek, K. T. Park, *ACS Sustain. Chem. Eng.* **2016**, *4*, 1311.
[16] D.-S. Huang, Y. Wang, Y. Tang, J.-R. Huang, P.-X. Li, C.-P. Liang, Z.-H. Zhao, P.-Q. Liao, X.-M. Chen, *Natl. Sci. Rev.* **2025**, *12*, nwaf329.
[17] P. Zhu, H. Wang, *Nat. Catal.* **2021**, *4*, 943.
[18] Y. Kang, T. Kim, K. Y. Jung, K. T. Park, *Catalysts* **2023**, *13*, 955.
[19] H. Yang, J. J. Kaczur, S. D. Sajjad, R. I. Masel, *J. CO2 Util.* **2017**, *20*, 208.
[20] L. Fan, C. Xia, P. Zhu, Y. Lu, H. Wang, *Nat. Commun.* **2020**, *11*, 3633.
[21] T. Zheng, C. Liu, C. Guo, M. Zhang, X. Li, Q. Jiang, W. Xue, H. Li, A. Li, C. W. Pao, J. Xiao, C. Xia, J. Zeng, *Nat. Nanotechnol.* **2021**, *16*, 1386.
[22] L. Lin, X. He, X. G. Zhang, W. Ma, B. Zhang, D. Wei, S. Xie, Q. Zhang, X. Yi, Y. Wang, *Angew. Chem., Int. Ed.* **2023**, *62*, 202214959.
[23] R. Nankya, Y. Xu, A. Elgazzar, P. Zhu, T. U. Wi, C. Qiu, Y. Feng, F. Che, H. Wang, *Angew. Chem., Int. Ed.* **2024**, *63*, 202403671.
[24] S. Guan, Z.-N. Chen, L.-Q. Liu, Y.-K. Li, C.-Y. Lan, J.-Z. Wang, P.-F. Yin, J. Yang, H. Liu, X.-W. Du, C. Dong, *ACS Appl. Energy Mater.* **2024**, *7*, 3201.
[25] C. Zhang, X. Hao, J. Wang, X. Ding, Y. Zhong, Y. Jiang, M. C. Wu, R. Long, W. Gong, C. Liang, W. Cai, J. Low, Y. Xiong, *Angew. Chem., Int. Ed.* **2024**, *63*, 202317628.
[26] Y. Kang, Y. Kim, Y. Doh, J. Lee, J. Kim, K. T. Park, *Angew. Chem., Int. Ed.* **2025**, *137*, 202504380.
[27] Z. H. Zhao, J. R. Huang, D. S. Huang, H. L. Zhu, P. Q. Liao, X. M. Chen, *J. Am. Chem. Soc.* **2024**, *146*, 14349.
[28] T.-U. Wi, Z. H. Levell, S. Hao, A. Elgazzar, P. Zhu, Y. Feng, F.-Y. Chen, W. P. Lam, M. Shakouri, Y. Liu, H. Wang, *ACS Energy Lett.* **2025**, *10*, 822.
[29] Y. Xia, P. Zhu, Y. Yang, C. Qiu, H. Wang, *ACS Catal.* **2025**, *15*, 4560.
[30] M. D. Zhang, J. R. Huang, C. P. Liang, X. M. Chen, P. Q. Liao, *J. Am. Chem. Soc.* **2024**, *146*, 31034.
[31] Y. C. Liu, J. R. Huang, H. L. Zhu, X. F. Qiu, C. Yu, X. M. Chen, P. Q. Liao, *Nat. Nanotechnol.* **2025**, *20*, 907.
[32] L. Hu, J. A. Wrubel, C. M. Baez-Cotto, F. Intia, J. H. Park, A. J. Kropf, N. Kariuki, Z. Huang, A. Farghaly, L. Amichi, P. Saha, L. Tao, D. A. Cullen, D. J. Myers, M. S. Ferrandon, K. C. Neyerlin, *Nat. Commun.* **2023**, *14*, 7605.
[33] L. H. Cherniack, K. U. Hansen, Z. Li, A. K. Taylor, K. C. Neyerlin, F. Jiao, *ACS Energy Lett.* **2025**, *10*, 1508.
[34] D. Joseph, J. Büsselmann, C. Harms, D. Henkensmeier, M. J. Larsen, A. Dyck, J. H. Jang, H.-J. Kim, S. W. Nam, *J. Membr. Sci.* **2016**, *520*, 723.
[35] M. Jung, W. Lee, N. Nambi Krishnan, S. Kim, G. Gupta, L. Komsiyska, C. Harms, Y. Kwon, D. Henkensmeier, *Appl. Surf. Sci.* **2018**, *450*, 301.
[36] H. Liu, Q. She, *J. Membr. Sci.* **2022**, *650*, 120398.
[37] M. Cho, S. Han, J. Jang, S. Choi, R. Kwak, B. Kim, *J. Membr. Sci.* **2025**, *717*, 123620.
[38] E. Moukheiber, G. De Moor, L. Flandin, C. Bas, *J. Membr. Sci.* **2012**, *389*, 294.
[39] Z. Bi, K. Li, C. Jiang, J. Zhang, S. Ma, C. Alberto, M. Sun, Y. Bu, M. Barati, S. Ren, *ACS Omega* **2022**, *7*, 21225.
[40] X. Song, Y. Wang, D. Song, C. An, J. Wang, *Nanomater. Nanotechnol.* **2016**, *6*, 23.
[41] D. Fein, *J. Catal.* **2002**, *210*, 241.
[42] B. Rutjens, K. von Foerster, B. Schmid, H. Weinrich, S. Sanz, H. Tempel, R.-A. Eichel, *Ind. Eng. Chem. Res.* **2024**, *63*, 3986.
[43] H. Yang, J. J. Kaczur, S. D. Sajjad, R. I. Masel, *J. CO2 Util.* **2020**, *42*, 101349.

© 2025 The Author(s). Advanced Science published by Wiley-VCH GmbH